Water and potassium dynamics inside the KcsA K^+ channel

Leonardo Guidoni[a], Vincent Torre[a], Paolo Carloni[a,b,*]

[a] *Istituto Nazionale per la Fisica della Materia (INFM), Italy and International School for Advanced Studies (SISSA), Via Beirut 4, 34014 Trieste, Italy*

[b] *International Centre for Genetic Engineering and Biotechnology, AREA Science Park, Padriciano 99, 34012 Trieste, Italy*

Received 10 March 2000; received in revised form 22 May 2000

Edited by Maurice Montal

Abstract Molecular dynamics simulations and electrostatic modeling are used to investigate structural and dynamical properties of the potassium ions and of water molecules inside the KcsA channel immersed in a membrane-mimetic environment. Two potassium ions, initially located in the selectivity filter binding sites, maintain their position during 2 ns of dynamics. A third potassium ion is very mobile in the water-filled cavity. The protein appears engineered so as to polarize water molecules inside the channel cavity. The resulting water induced dipole and the positively charged potassium ion within the cavity are the key ingredients for stabilizing the two K^+ ions in the binding sites. These two ions experience single file movements upon removal of the potassium in the cavity, confirming the role of the latter in ion transport through the channel.

Key words: KcsA; Potassium channel; Potassium ion; Molecular dynamics; *Streptomyces lividans*

1. Introduction

The recent determination of the crystal structure of a bacterial potassium channel (Kcsa from *Streptomyces lividans*) [1] has provided the molecular basis to understand the physical mechanisms controlling ionic selectivity, permeation and transport through K^+ channels [2–4]. Indeed, although this channel is gated by pH [5–8] and not by voltage as most K^+ channels [9], its ionic selectivity and its single channel conductance is representative of more complex potassium channels.

The X-ray structure [1] has revealed the existence of three binding sites within the channel selectivity filter region, occupied by two potassium ions and water (Fig. 1A) and of a water-filled cavity [1,10], which significantly reduces the region inside the channel where the ion needs dehydration.

Theoretical approaches based on this structure [11–15] or on simplified structural models [16,17] are also of invaluable help in uncovering important aspects of ion transport. In particular, molecular dynamics (MD) simulations [14] have shown that the channel is engineered so as to catalyze the dehydration step of permeating ions: the dehydration process is therefore likely not to be a rate limiting step, in contrast to previous proposals [4]. Furthermore, these simulations have led to the suggestion that ion permeation is possibly related to breathing motions of the intracellular mouth of the protein [15]. Electrostatic modeling based on the Poisson–Boltzmann (PB) equation [18], on the other hand, has emerged as a complementary computational tool for understanding structure–function relationships in the channel. These calculations have indicated that the pore helix electrostatic field is crucial for the selectivity for monovalent cations in the cavity [11].

In this paper, we address fundamental questions about the stability of the potassium ions within the channel pore and water dynamics inside the KcsA channel. Both theoretical approaches are used to understand key factors stabilizing the potassium ions in the selectivity filter binding sites, as found by the X-ray structure.

Anticipating our results, we find that water polarization, due to the protein environment and potassium mobility within the cavity, controls ion–ion interactions inside the KcsA channel, and therefore ion transport.

2. Materials and methods

2.1. Structural models

Our models **3K** and **2K** were based on the crystal structure of the Kcsa potassium channel from *S. lividans* [1] (Protein Data Bank (PDB) [19,20] accession number 1BL8). Groups missing in the X-ray structure (Arg-27, Ile-60, Arg-64, Glu-71, Arg-117) were added as in [14][1]. The presence of a solvated pore inside the channel, already deduced by the X-ray structure [1], has been directly confirmed by a site-directed spin labeling study [10].

Water and potassium ions were added as follows. In both **3K** and **2K** models, two potassium ions ($K^+_{(1)}$ and $K^+_{(2)}$) were located in the selectivity filter in the outer ($K^+_{(1)}$, see Fig. 1A) and middle ($K^+_{(2)}$) crystallographic binding sites and separated by an ordered, crystallographic water molecule (WAT) [1]. It has been suggested that the cavity accommodates one potassium ion [11]. This ion ($K^+_{(3)}$) was added in model **3K**. Following [11], $K^+_{(3)}$ (not present in the coordinate PDB file [1]) was positioned in the water cavity along the channel axis, 8 Å from Thr-74 carbonyl oxygens. Subsequently, the cavity of the channel was filled with water molecules [10] (31 and 30 for **2K** and **3K**, respectively)[2]. Finally, the systems were immersed in an equilibrated water–*n*-octane ($\approx 69\times65\times66$ Å^3) box. This approach supplies a stable hydrophilic–hydrophobic liquid interface quickly adaptable to

*Corresponding author: Fax: (39)-40-3787 528.
E-mail: carloni@sissa.it

Abbreviations: MD, molecular dynamics; **2K**, model with two potassium ions; **3K**, model with three potassium ions; rmsd, root mean square displacement

[1] Glu-71 side chain may be assumed either deprotonated (a), thus interacting with Tyr-78 and Gly-79 [14], or protonated (b) [11], sharing the proton with Asp-80 and H-bonding to Tyr-78. Moreover, as MD simulations for the two protomers turned out to provide very similar results, for sake of simplicity only calculations based on (b) are reported here.

[2] Simulations carried out with a larger number of water molecules [11] (50 and 51 for **2K** and **3K**, respectively) turn out to give similar water content at the end of the simulations (see Section 3), as well as very similar results, and therefore they are not reported here.

0014-5793/00/$20.00
PII: S0014-5793(00)01712-9

the protein and has been successfully applied in literature to transmembrane channel models [21] and to KcsA [14]. As in previous work [14,22,23], the water–hydrocarbon interfaces were located between Trp-87 and Thr-85 (extracellular side) and between Trp-113 and Arg-117 (intracellular side). This choice, suggested by Doyle et al. [1], turns out to be in excellent agreement with recent EPR data [10].

2.2. Potassium chloride in water

A K^+ ion and a Cl^- ion were immersed in a cubic box ($\approx$40 Å edge) of Monte Carlo water [24]. At least 10 water molecules interposed between the two ions in the starting configuration.

2.3. Computational setup

Force field parameters, as well as the MD conditions, were the same as [14]. In particular, periodic boundary conditions were applied and electrostatic interactions were calculated with the particle mesh Ewald summation [25].

2.4. MD calculations

All MD calculations were carried out using the AMBER 5.0 suite of programs [24].

The MD simulation of **3K** was carried out as follows. The bilayer, the protein hydrogens and $K^+_{(3)}$ were equilibrated for 0.1 ns at 298 K. $K^+_{(3)}$ motion was weakly restrained by imposing a harmonic restrain on its starting position (force constant = 0.5 kcal/(mol Å^2)). After this procedure, the resulting thickness of the octane layer, turned out to be $\approx$33 Å. Then, the whole system was heated up by performing MD runs (of 15 ps each) at 50, 100, 150, 200, 250 and 298 K. Finally, 2.0 ns of dynamics at room temperature was carried out, and the last 1.4 ns were collected for analysis. The final MD structure is available through anonymous ftp at ftp://masaccio.cm.sissa.it.

Two **2K** MD runs were carried out. The first was as **3K**, except that only 0.5 ns of MD simulation at room temperature were collected. The second run was as the first, except that the $K^+_{(1)}$- and $K^+_{(2)}$-donor atom distances were restrained during the first 130 ps of MD (force constant = 5 kcal/(mol Å^2)).

For potassium chloride in water, 0.5 ns of MD were carried out at room temperature, of which 0.4 ns were collected for analysis. At least 10 water molecules were interposed between the two ions during the dynamics.

2.5. Calculated properties

(i) Root mean square displacements (rmsd's) were calculated as in [26]. (ii) Radial $g(r)$ and angular $g(\theta)$ distribution functions (dfs) were calculated as in [27]. Water $g(\theta_{OH-O})$ was calculated up to d(H–O) = 2.5 Å, that is the distance corresponding to the first minimum of $g(r_{O-H})$ in bulk water [28]. (iii) K^+ coordination numbers were calculated by integrating $g(r_{K^+-O})$ up to its first minimum at 3.65 Å [29]. These numbers take into account also the coordination bond with Thr-75 carbonyl oxygens, which turned out to replace up to four water molecules for $\sim$35% of simulated time. (iv) The pore radius profile was calculated with the HOLE program [30]; its integral provided the pore volume. (v) The water electric dipole was calculated from the TIP3P water model partial atomic charges [28]. (vi) Calculations of electric fields along the channel axis for (a) the protein-$K^+_{(1)}$–$K^+_{(2)}$ adduct and (b) the four pore helices (residues 62–74) were based on RESP partial atomic charges [31]. A simple point charge (PC) model in vacuo (dielectric constants $\varepsilon = 1$) as well as the PB model [32,33] ($\varepsilon = 78$ and $\varepsilon = 2$ for water and for the protein, respectively) were used. In model (b) all charges other than the pore helices atoms were turned off. (vii) $K^+_{(2)}$–Water and $K^+_{(2)}$–$K^+_{(3)}$ electrostatic interaction energies were calculated during the dynamics every 6 ps using the same simple PC model as above. The Thr-75 side chain, which has been shown solvating frequently $K^+_{(3)}$ (see iii) was considered in this calculation as belonging to the cavity solvent.

All molecular structures were drawn using the VMD program [34].

3. Results

In this section we analyze the structural and dynamical properties of the adduct with three potassium ions (**3K**). Comparison is then made with the adduct without $K^+_{(3)}$ in the channel cavity (**2K**).

*3.1. Protein structure and dynamics of **3K***

During the simulation, the channel structure is rather stable: indeed α-helix hydrogen bond patterns as well as subunit–subunit contacts are well preserved in the ns time scale. Structures sampled every 0.15 ns exhibit a fairly good Ramachandran plot [35][3]. The protein is also well equilibrated. After $\approx$0.6 ns, the rmsd fluctuates around the average value of 2.7(1) Å (2.1(1) Å for backbone atoms). In the sub-ns timescale, Asp-80 and Arg-89 belonging to neighboring subunits form and break salt bridges not emerging from the X-ray structure [1]. These interactions provide large contributions to the stabilization of the channel structure and they have been extensively analyzed in our previous simulation [14]. Asp-80 also maintains its H-bond with protonated Glu-71, the average O_δ(Asp-80)–O_δ(Glu-71) distances in the four subunits ranging from 2.6(1) to 2.8(2) Å.

The geometrical properties of the channel pore can be described by the pore radius profile [30]. The MD-averaged pore radius belonging to the region occupied by internal water and K^+ is very similar to that of the X-ray structure [1]. Consistently, the volumes, calculated over these regions, are rather similar (397 Å^3 and 486 Å^3, for the MD and the X-ray structure, respectively).

Thus, force field parameterization used in this work appears to reproduce well the structural features of the protein.

3.2. Mobility of the potassium ions

The three K^+ ions remain in their initial binding site in the ns time scale investigated (Fig. 1). However, their mobility is markedly different: $K^+_{(1)}$ and $K^+_{(2)}$ experience small fluctuations around their average positions (the rmsd's along the channel axis = 0.3 Å for both ions). In contrast, $K^+_{(3)}$ is very mobile (rmsd 1.9 Å), its ensemble of positions being fully consistent with the diffuse experimental electronic density inside the channel cavity [1].

$K^+_{(3)}$ is highly hydrated. However, it spends a significant portion of the simulated time binding also to some or all of the four Thr-75 O_γ oxygen atoms. Comparison of the MD-averaged coordination number (6.8(0.9)) with that of KCl in bulk water (6.9(1.0)) shows that the potassium coordination shell is similar to that of potassium in water.

3.3. Internal hydration of the channel

While WAT maintained its position during the dynamics, five water molecules left the channel cavity during the system equilibration, and diffused toward the hydrophobic layer and bulk water within 0.2 ns. Water diffuses to a greater extent if a larger water content is initially present in the channel cavity (see footnote 2 in Section 2.1). As a result, a similar amount of water was present at the end of both dynamics (2 ns). Thus, the channel appears to accommodate between 20 and 30 water molecules inside the cavity.

The structural properties of water are conveniently compared to those of bulk water through analysis of g_{OO}, g_{OH} radial and g_{OH-O} angular dfs. While the radial dfs are barely similar (data not shown), small but significant discrepancies

[3] In one subunit, Val-76 backbone rearranges after $\approx$0.1 ns to a different conformation, which also exhibits a good Ramachandran plot [35] (From $\varphi,\Psi = -122, -25$ to $\varphi,\Psi = -127, 141$). As a result, WAT replaces the Val-76 carbonyl group in the coordination sphere of $K^+_{(2)}$ for the rest of the simulation.

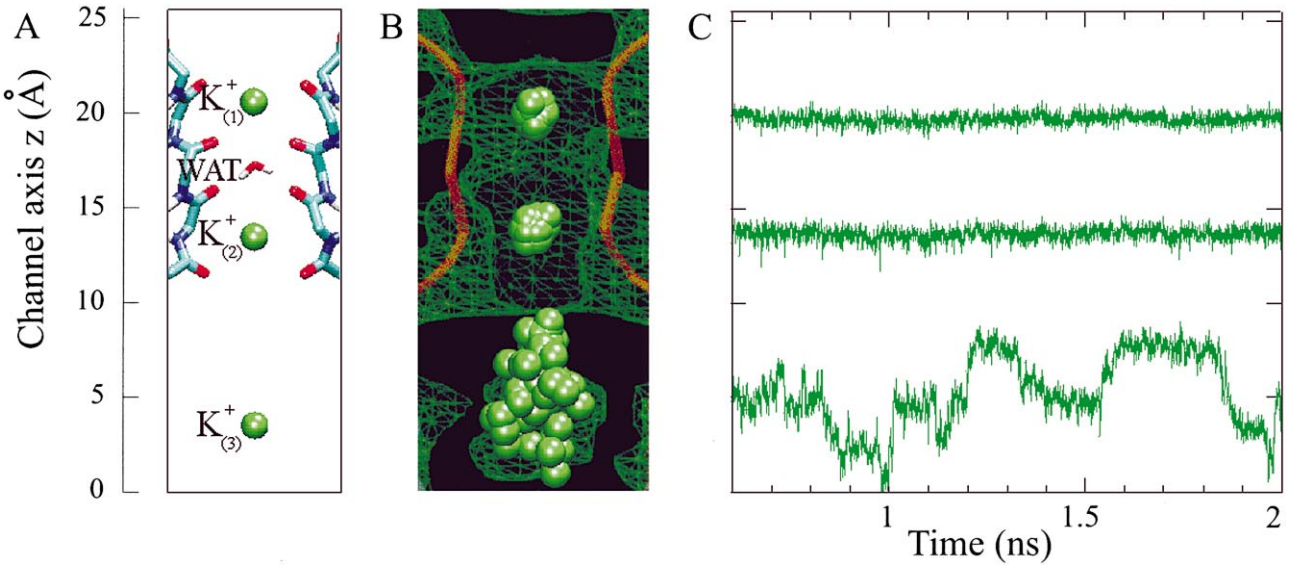

Fig. 1. Structure and mobility of potassium ions (green). A: Location and labeling of the ions and of the crystal water. The position along the channel axis is also shown. The origin is set arbitrarily. B: Scatter plot of K^+ positions during the production dynamics displayed every 50 ps. The experimental density map (1 σ contoured) and the backbone trace (yellow) are also displayed with permission from reference [1]. C: Ion motion on the channel axis plotted as a function of time.

are found between the two g_{OH-O}'s: the channel water g_{OH-O} is broader and exhibits a smaller maximum than that of the bulk. Visual inspection of the water network confirms that water in the cavity is structured differently from the bulk water. A typical MD snapshot (Fig. 2A) shows that the water c_2 symmetry axes are partially aligned along the axis channel (z-coordinate).

An important consequence of this alignment is the formation of a large dipole D directed essentially along the z-axis (see Fig. 2A). D points towards the extracellular side during most of the simulation, although it experiences large fluctuations. Fig. 2B shows that the z-component (D_z) oscillates from more than 30 Debye to zero and even to negative values, that is D pointing toward the intracellular side.

Water molecules are not polarized uniformly in the cavity. The largest polarization is found in the region close to the extracellular side (Fig. 2C). There, the dipole–molecule contribution along the z-axis reaches 2.0 Debye, that is ∼85% of TIP3P water dipole [28].

What are then the important factors responsible for the strong water polarization and of its large fluctuations in time?

Inspection of crystal and MD structures points to the four pore helices as key factors for water polarization, as their COOH termini point toward the channel cavity from the extracellular side [11] (Fig. 3). Electrostatic calculations, based either on a simple PC model or on the PB equation [32,33], show that the helix field accounts for more than three quarters of the field of the protein, with a magnitude of the order of 10

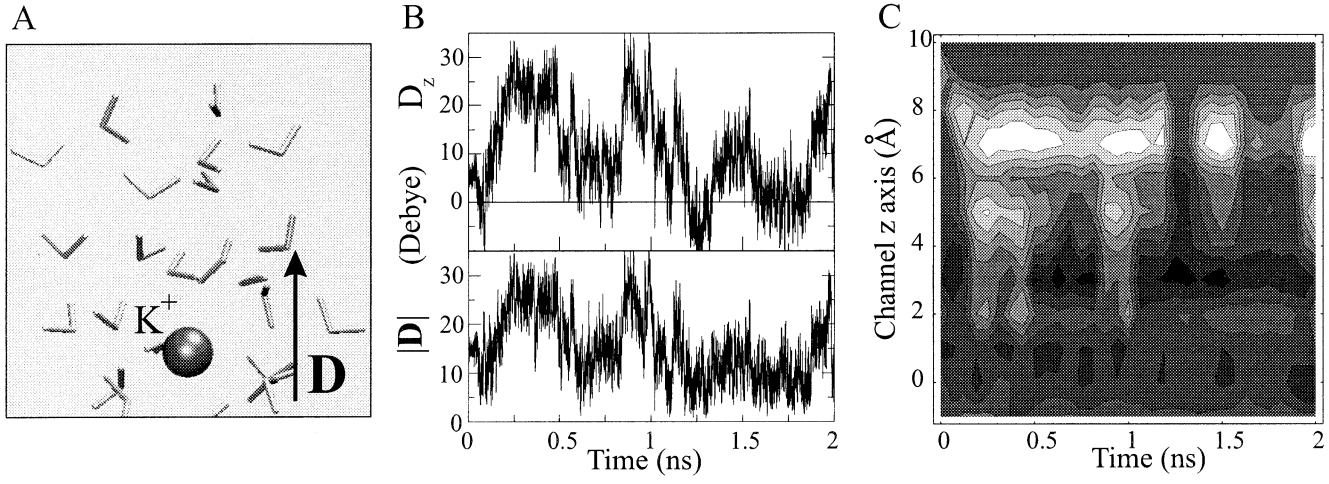

Fig. 2. Electric dipole momentum of the water inside the channel. A: Representative snapshot of water polarization at 0.9 ns. B: The inner water total dipole |D| and its component along the channel axis D_z plotted as a function of the simulated time. Almost all contribution to |**D**| arises from D_z. C: D_z fluctuations during the dynamics are plotted as a function of channel axis and simulated time. Lighter regions correspond to D_z orientation towards the extracellular side. Contours range from −2 Debye/Å (black) to +5 Debye/Å (white). Scale of the z-axis is consistent to that shown in Fig. 1.

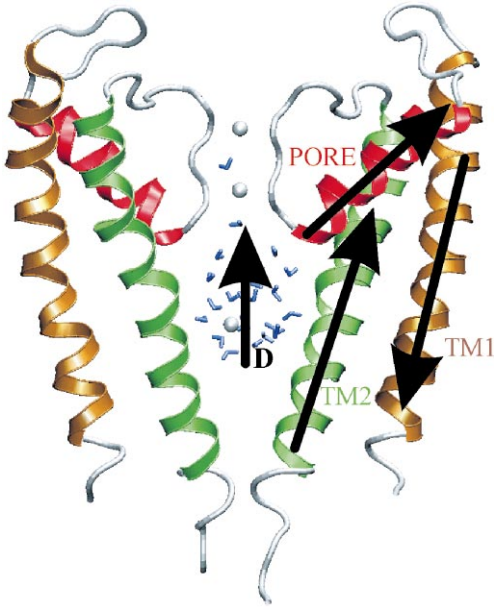

Fig. 3. Water-helices dipole–dipole electrostatic interactions. Dipole momenta are sketched as black arrows. The role of the pore helix for water polarization is apparent from the relative orientation of D and the helix dipoles.

(PB) to 100 (PC) mV/Å. Furthermore, the field increases on approaching the extracellular side of the channel, consistent with the polarization plot shown in Fig. 2C.

The electrostatic modeling also shows that the two transmembrane helices TM1 and TM2 do not provide a significant contribution to water polarization. Indeed, their effect almost cancels out, because their large dipoles have an antiparallel orientation (Fig. 3).

The large fluctuations of the total water dipole must arise from large rearrangements or fast motions of interacting groups. In this respect, $K^+_{(3)}$ is putatively important because of its high mobility inside the cavity. That this is indeed the case is shown by the strong correlation between the ion position along the channel z-axis with D_z magnitude (Fig. 4). Three regimes can be identified: when $K^+_{(3)}$ is close to the extracellular side ($z > 6$ Å, the scale from Figs. 1, 2 and 4), D_z is zero or even negative (Fig. 4, upper region); instead, when $K^+_{(3)}$ is located near the intracellular side ($z < 4$ Å), D_z is positive and very large (Fig. 4, lower region); finally, when

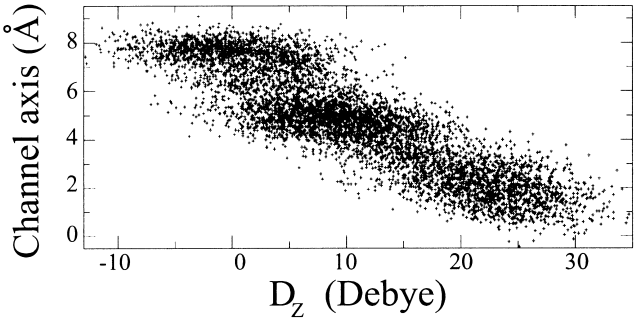

Fig. 4. Correlation plot between water dipoles D_z and the $K^+_{(3)}$ positions along the axis channel. The scale of the axis is consistent with Figs. 1 and 2.

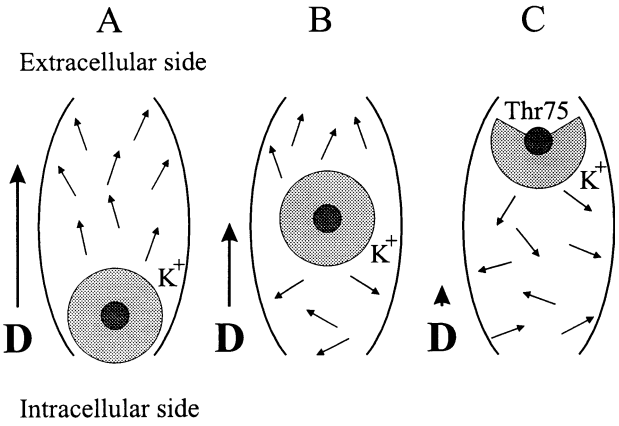

Fig. 5. Interplay between $K^+_{(3)}$ dynamics and water polarization inside the cavity. Each cartoon includes water single (thin arrows) and total (thick arrow) D dipoles as well as $K^+_{(3)}$ and its first hydration shell (dark and light gray spheres, respectively). D, large and directed towards the extracellular side in (A), decreases dramatically when $K^+_{(3)}$ moves to the center (B), becoming small or negative when the ion is located in the top (C) of the cavity. When $K^+_{(3)}$ is located close to the extracellular side (C), it can bind to Thr-75 O_γ atoms (average coordination number 2.6(0.9)).

$K^+_{(3)}$ is found in the center of the cavity ($4 \leq z \leq 6$ Å), D_z assumes intermediate values (Fig. 4, middle region).

An explanation of the dynamic influence of $K^+_{(3)}$ on water polarization is offered by its hydration properties. Although the first hydration shell of $K^+_{(3)}$ provides essentially a zero net contribution to D, the outer-sphere hydration properties do affect water polarization (Fig. 5). When $K^+_{(3)}$ is located at the bottom of the cavity, it tends to orient all the water dipoles but those directly bound towards the extracellular side (Fig. 5A). Thus, the net effect of $K^+_{(3)}$ adds to that of the pore helix dipoles, and D is very large. When $K^+_{(3)}$ moves towards the cavity center, its polarization effects are approximately isotropic also on the outer-shell spheres, as in bulk water. Thus, it provides a negligible contribution to water polarization. As a consequence, D is considerably smaller but still significant because of the pore helix field (Fig. 5B). Finally, when $K^+_{(3)}$ is located near the extracellular side, it tends to polarize the water dipoles so as to counterbalance that in-

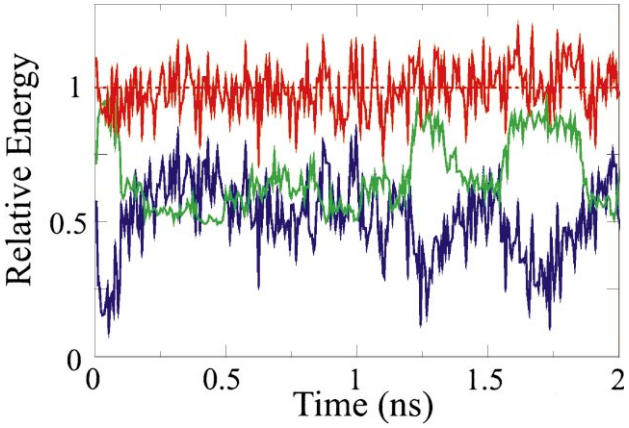

Fig. 6. Electrostatic force field based interaction energies between $K^+_{(2)}$/ and the ($K^+_{(3)}$–water) systems in the channel cavity. $K^+_{(2)}$–cavity (blue), $K^+_{(2)}$–$K^+_{(3)}$ (red), and $K^+_{(2)}$–inner water (green) energies are plotted as a function of simulated time. Energy values are expressed in units of average $K^+_{(2)}$–cavity interaction (65 kcal/mol).

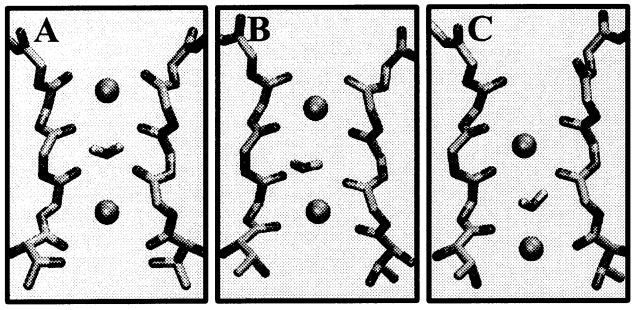

Fig. 7. Dynamics of $K^+_{(1)}$, $K^+_{(2)}$ ions. The figures show the alkali ions (spheres), the crystallographic water and the backbone of two opposite subunits of the selectivity filter (sticks). A: X-ray structure and snapshots after 190 ps of **3K** (B) and **2K** (C), respectively.

duced by pore helix dipoles, leading to a dramatic reduction of D. The net result is that water is not polarized in the channel cavity (Fig. 5C).

In summary, the pore helix dipoles generate the electric field responsible for the strong water polarization, which fluctuates widely because of the high mobility of the potassium ion inside the cavity (Figs. 3–5).

These findings can provide a rationale for the stability and the relatively low mobility of two potassium ions in the binding sites. Because D points towards $K^+_{(2)}$, the electrostatic interaction between $K^+_{(2)}$ and the potassium–water system is expected to be repulsive and therefore might prevent $K^+_{(2)}$ (and hence $K^+_{(1)}$) to diffuse inside the channel. Indeed, the calculated $K^+_{(2)}$–cavity interaction energy is positive and much larger than kT (of the order of several tens of kcal/mol[4]). Furthermore, it is almost constant over the entire simulation (Fig. 6). This result is apparently surprising because $K^+_{(3)}$ fluctuates very widely in the channel cavity (its motion along the axis channel ranges over 7 Å). However, because of the correlation between $K^+_{(3)}$ position and water polarization (Figs. 4 and 5), the $K^+_{(2)}$–$K^+_{(3)}$ and the $K^+_{(2)}$–water interaction energies compete to each other. When $K^+_{(3)}$ is close to $K^+_{(2)}$ (top of cavity channel, Fig. 5C), it provides most of the electrostatic repulsion. In contrast, when $K^+_{(3)}$ is far from $K^+_{(2)}$ (Fig. 5A), ion–ion repulsion is drastically reduced and D provides a fundamental contribution to the repulsion energy.

Would this dynamical equilibrium of the channel be broken if one of the ingredients was missing? To answer this question, we follow the dynamics of a system in which $K^+_{(3)}$ is removed. MD simulations carried out on the **2K** model in rather different conditions (see computational details) provide invariably the same picture: the two $K^+_{(1)}$ and $K^+_{(2)}$ ions experience a single file movement towards the channel cavity within the first 0.2 ns of simulation (Fig. 7). As a result, $K^+_{(1)}$ and $K^+_{(2)}$ occupied the WAT and the more intracellular crystallographic binding sites, respectively. Thus, removal of $K^+_{(3)}$ is reflected in an immediate instability of the system.

4. Discussion and conclusion

Our calculations indicate that the water molecules within the channel cavity are significantly polarized by the four pore helix dipoles. This finding is fully consistent with a recent EPR study, which points to the discrepancies between water penetrating the channel and that in the bulk [10]; furthermore, it agrees with previous MD studies, which reveal the role of secondary structure elements for the polarization of the inner solvent on α-helix boundless ion channels [36–38].

Water molecules are expected to be polarized also in the presence of the physiological membrane potential. Indeed, the calculated pore helix electric field is much larger ($\sim$0.01–$\sim$0.1 V/Å, depending on the electrostatic model used) than that present in physiological conditions, where $\sim$100 mV potential is applied to membranes some nm width.

Water polarization causes the formation of a large dipole D along the channel axis, directed towards the extracellular side (Fig. 3). D fluctuates widely because of the electric field of the positively charged, highly mobile $K^+_{(3)}$ cation.

Our MD simulations show that the K^+ ions remain in their initial sites (although they differ markedly in mobility (Fig. 1)), consistently with X-ray structural data [1], which suggests the presence of two potassium ions in the selectivity filter.

Electrostatic modeling suggests that the mechanism preventing rapid ion transport in the channel is based on the interaction between $K^+_{(2)}$ and the $K^+_{(3)}$–water system. This interaction is repulsive as D points towards $K^+_{(2)}$ (Fig. 3). It is very large (of the order of tens kcal/mol in a PC model) because of the large magnitude of D and the large $K^+_{(2)}$–$K^+_{(3)}$ repulsion. Finally, it is almost constant (that is, not dependent on $K^+_{(3)}$ position) as $K^+_{(2)}$–$K^+_{(3)}$ and $K^+_{(2)}$–D interactions compete to each other during the dynamics (Fig. 6): when $K^+_{(3)}$ is close to the intracellular mouth, its electric field further polarizes the water molecules (Fig. 5A) and D is close to its maximum value ('saturation regime'). In this case, both $K^+_{(2)}$–D and $K^+_{(2)}$–$K^+_{(3)}$ interactions play a fundamental role for $K^+_{(2)}$ stabilization. In contrast, when $K^+_{(3)}$ is close to the selectivity filter, it generates a field just opposite to that induced by the pore helices: D is zero or even negative (Fig. 5C). In this case, $K^+_{(2)}$–$K^+_{(3)}$ interaction energy is very large and it represents the essential ingredient for $K^+_{(2)}$ stabilization.

The essential role of the water–$K^+_{(3)}$ system is confirmed by simulations carried out without $K^+_{(3)}$. $K^+_{(1)}$ and $K^+_{(2)}$ do not remain in their original binding sites and have a single file movement towards the inner vestibule within a few hundred ps.

Departure of the $K^+_{(3)}$ ion from the central cavity to its intracellular mouth (for instance as a consequence of a 'breathing' motion [15] of the channel) may be a basic feature of channel gating. The present mechanism is at the speculative level, yet it is encouraging that, in a recent MD simulation of the potassium channel in a phospholipid bilayer, the exit of a potassium upon enlargement of the intracellular mouth triggers ion transport through the channel [15].

In summary, two important features can be drawn from the present study. First, the protein is engineered so as to polarize water molecules inside the channel cavity, thus inducing a large dipole. Second, this dipole and the positively charged potassium ion inside the channel $K^+_{(3)}$ stabilize the two ions in the binding sites (and thus inhibiting ion transport) in a concerted and dynamical mechanism. Because solvent continuum models cannot describe this mechanism, explicit treatment of the solvent appears necessary to describe correctly gating, ion permeation and selectivity. The high homology between KcsA and eukaryotic voltage-gated channels may

[4] Exact values must be taken with caution as they are based on a simple force field calculation.

extend the domain of these conclusions to this important class of channels [39].

Acknowledgements: We thank A. Laio, D. Lamba and S. Piana, for useful discussions, D. Frigyes and P. Tangney for their help. This work was supported by a Biotechnology Grant from EC (No. 960593) and by the Ministero dell' Università e della Ricerca Scientifica e Tecnologica (M.U.R.S.T.-COFIN).

References

[1] Doyle, D.A., Morais, C.J., Pfuetzner, R.A., Kuo, A., Gulbis, J.M., Cohen, S.L., Chait, B.T. and MacKinnon, R. (1998) Science 280, 69–77.
[2] Heginbotham, L. (1999) Nat. Struct. Biol. 6, 811–814.
[3] Hille, B., Armstrong, C.M. and MacKinnon, R. (1999) Nat. Med. 5, 1105–1109.
[4] Hille, B. (1992) Ionic Channels of Excitable Membranes, Sinauer Associates.
[5] Cuello, L., Romero, J.G., Cortes, D.M. and Perozo, E. (1998) Biochemistry 37, 3229–3236.
[6] Perozo, E., Cortes, D.M. and Cuello, L.G. (1999) Science 285, 73–78.
[7] Heginbotham, L., LeMasurier, M., Kolmakova-Partensky, L. and Miller, C. (1999) J. Gen. Physiol. 114, 551–560.
[8] Meuser, D., Splitt, H., Wagner, R. and Schrempf, H. (1999) FEBS Lett. 462, 447–452.
[9] Catterall, W.A. (1995) Annu. Rev. Biochem. 64, 493–531.
[10] Gross, A., Columbus, L., Hideg, K., Altenbach, C. and Hubbell, W.L. (1999) Biochemistry 38, 10324–10335.
[11] Roux, B. and MacKinnon, R. (1999) Science 285, 100–102.
[12] Aqvist, J. and Luzhkov, V. (2000) Nature 404, 881–884.
[13] Bernèche, S. and Roux, B. (2000) Biophys. J., in press.
[14] Guidoni, L., Torre, V. and Carloni, P. (1999) Biochemistry 38, 8599–8604.
[15] Shrivastava, I.H. and Sansom, M.S. (2000) Biophys. J. 78, 557–570.
[16] Allen, T.W., Kuyucak, S. and Chung, S.H. (1999) Biophys. J. 77, 2502–2516.
[17] Chung, S.H., Allen, T.W., Hoyles, M. and Kuyucak, S. (1999) Biophys. J. 77, 2517–2533.
[18] Honig, B. and Nicholls, A. (1995) Science 268, 1144–1149.
[19] Sussman, J.L., Lin, D., Jiang, J., Manning, N.O., Prilusky, J., Ritter, O. and Abola, E.E. (1998) Acta Cryst. D 54, 1078–1084.
[20] Abola, E.E., Sussman, J.L., Prilusky, J. and Manning, N.O. (1997) Methods Enzymol. 277, 556–571.
[21] Zhong, Q., Moore, P.B., Newns, D.M. and Klein, M.L. (1998) FEBS Lett. 427, 267–270.
[22] Moore, P.B., Zhong, Q., Husslein, T. and Klein, M.L. (1998) FEBS Lett. 431, 143–148.
[23] Zhong, Q., Husslein, T., Moore, P.B., Newns, D.M., Pattnaik, P. and Klein, M.L. (1998) FEBS Lett. 434, 265–271.
[24] Case, D.A., Pearlman, D.A., Caldwell, J.W., Cheatham III, T.E., Ross, W.S., Simmerling, C.L., Darden, T.A., Merz, K.M., Stanton, R.V., Cheng, A.L., Vincent, J.J., Crowley, M., Ferguson, D.M., Radmer, R.J., Seibel, G.L., Singh, U.C., Weiner, P.K., and Kollman, P.A. (1997) AMBER 5.
[25] Essman, U., Perera, L., Berkowitz, M.L., Darden, T., Lee, H. and Pedersen, L.G. (1995) J. Chem. Phys. B 103, 8577–8593.
[26] McLachlan, A.D. (1979) J. Mol. Biol. 128, 49–79.
[27] Allen, M.P. and Tildesley, D.J. (1987) Computer simulations of liquids, Oxford university Press, Oxford.
[28] Jorgensen, W.L., Chandrasekhar, J. and Madura, J.D. (1983) J. Chem. Phys. 79, 926–935.
[29] Song, H.L. and Jayendran, C.R. (1996) J. Phys. Chem. 100, 1420.
[30] Smart, O.S., Neduvelil, J.G., Wang, X., Wallace, B.A. and Sansom, M.S. (1996) J. Mol. Graph. 14, 354–376.
[31] Cornell, W.D., Cieplack, P., Bayly, C.I., Gould, I.R., Merz, K.M., Ferguson, D.M., Spellmeyer, D.C. and Fox, T. (1995) J. Am. Chem. Soc. 117, 5179–5197.
[32] Honig, B. and Nicholls, A. (1995) Science 268, 1144–1149.
[33] Gilson, M.K., Sharp, K.A. and Honig, B.H. (1987) J. Comp. Chem. 9, 327–335.
[34] Humphrey, W., Dalke, A. and Shulten, K. (1996) J. Molec. Graph. 14, 33–38.
[35] Morris, A.L., MacArthur, M.W., Hutchinson, E.G. and Thornton, J.M. (1992) Proteins 12, 345–364.
[36] Breed, J., Sankararamakrish, R., Kerr, I.D. and Sansom, M.S.P. (1996) Biophys. J. 70, 1643–1661.
[37] Sansom, M.S., Smith, G.R., Adcock, C. and Biggin, P.C. (1997) Biophys. J. 73, 2404–2415.
[38] Tieleman, D.P., Berendsen, H.J. and Sansom, M.S. (1999) Biophys. J. 76, 1757–1769.
[39] MacKinnon, R., Cohen, S.L., Kuo, A., Lee, A. and Chait, B.T. (1998) Science 280, 106–109.